Progress In Electromagnetics Research, Vol. 133, 425–441, 2013

INVESTIGATION ON THE SCATTERING FROM ONE-DIMENSIONAL NONLINEAR FRACTAL SEA SURFACE BY SECOND-ORDER SMALL-SLOPE APPROXIMATION

G. Luo and M. Zhang*

School of Science, Xidian University, Xi'an 710071, China

Abstract—In this paper, a one-dimensional nonlinear fractal sea surface model has been established based on the narrow-band Lagrange model, which takes into account the vertical and horizontal skewnesses for the sea surface. By using the method of second-order small-slope approximation (SSA-II), the normalized radar cross section (NRCS) and Doppler spectrum of linear and nonlinear fractal sea surface are calculated. The calculated NRCS of the nonlinear fractal sea surface is larger than the linear surface for backscattering, especially for large incidence angles, which indicates the nonlinear surface has stronger scattering echoes. And the result of nonlinear fractal sea surface is also larger than the linear fractal sea surface for bistatic case, which is characterized as the discrepancies being small near specular direction, while the discrepancies becoming larger as the scattering angles departing from the specular direction. For the Doppler spectrum of sea surface, the nonlinearity of sea surface effects greatly enhances the Doppler shift and the Doppler spectrum bandwidth at large incidence angles, which are attributed the fact that the nonlinear-wave components propagate faster than the linear-wave components and the nonlinear fractal sea surface corrects the phase velocities by adding the horizontal and vertical skewness. And also, all the results can indicate the validity of this nonlinear model.

1. INTRODUCTION

The study of electromagnetic (EM) scattering from sea surfaces is an old but vigorous research realm. Stochastic waves can be used to form a rough sea surface, and has been widely applied to the research areas such as oceanic surveillance, target detection [1–8], remote sensing and

Received 27 August 2012, Accepted 25 October 2012, Scheduled 1 November 2012
* Corresponding author: Min Zhang (mzhang@mail.xidian.edu.cn).

so on [9–15]. But the fractal sea surface is also a very good tool for characterizing the natural sea surface as a result of its semi-stochastic and semi-periodic features [16, 17]. So far, a lot of fractal sea surface models have been applied to the study of EM scattering from rough surfaces [18–25]. Most of the models are linear sea surfaces, and the Kirchhoff approximation (KA) is usually employed to analyze the EM scattering problems.

However, the real surface is usually nonlinear and the EM scattering of the nonlinear sea surface might have a big difference from the linear surface, especially for Doppler spectrum. A nonlinear fractal sea surface is developed in [24, 26] by applying the two-scale method of Longuet-Higgins and Stewart and the backscattering coefficients discrepancies between linear and nonlinear models are observed. Yet, there is no more information in [24, 26] about the discrepancies of the time-varying signals, and the nonlinearity of sea surface might have great effect on the time-dependent signals such as Doppler spectrum according to some recently published researches about the scattering from nonlinear sea surfaces [27–29], so it is necessary to establish another nonlinear fractal sea model, which should be able to carry more signals scattering from rough surfaces.

A one-dimensional nonlinear fractal sea surface model has been established based on the narrow-band Lagrange model in this paper, in which the vertical and horizontal skewnesses are both considered [30–32]. In fact, this model has been used to study the Doppler spectrum of sea surface by Wang et al. in [32], but the method used in [32] is two-scale method, which can not calculate the scattering field directly from linear and nonlinear sea surfaces. Accounting for this problem and the shortages of KA, the method of SSA-II is employed to calculate the scattering field of fractal sea surface in this paper. The SSA-II method is developed by Voronovich [33, 34] and has been widely applied to analyze the EM scattering from sea surfaces [27, 35], which can reach an enough accurate electromagnetic description.

We would like to exhibit the influence of nonlinearity on the EM scattering from fractal sea surface in this paper. In Section 2, the one-dimensional nonlinear fractal sea surface is established by using the model of narrow-band Lagrange. Section 3 presents the model of SSA-II scattering from one-dimensional fractal sea surface detailed, and the results of backscattering, bistatic scattering and Doppler spectrum of linear and nonlinear fractal sea surface are displayed in Section 4. Some conclusions are presented in the final section.

2. NONLINEAR FRACTAL SEA SURFACE MODEL

A linear fractal sea surface model is represented as follows [23, 25, 36]:

$$f(x,t) = \sigma C \sum_{n=0}^{N_f-1} b^{(s-2)n} \sin\left[K_0 b^n (x+Vt) - \omega_n t + \phi_n(t)\right] \quad (1)$$

where σ is the standard deviation of the sea wave amplitude, C the normalization constant, s the fractal dimension ($1 \leq s \leq 2$), K_0 the fundamental spatial wavelength, $b\,(b > 1)$ the scale factor, V the observer platform velocity, ω_n the angular frequency, and N_f the number of sinusoidal components.

The phase $\phi_n(t)$ are stochastic and are set according to the following relationship:

$$\phi_n(t) = \begin{cases} \varphi_n & 0 \leq n \leq n_0 - 1 \\ \psi_n(t) & n_0 \leq n \leq N_f - 1 \end{cases} \quad (2)$$

where φ_n, $\psi_n(t)$ are independent random variables, which are uniformly distributed between $[-\pi, \pi]$. $\psi_n(t)$ are time-varying. In order to ensure spatial correlation of fractal sea surface varying with time and calculate the Doppler spectrum, $\psi_n(t)$ are set time invariant in a short time interval.

The linear fractal sea surface can be rewritten as

$$\begin{aligned} f(x,t) &= \sum_{n=0}^{N_f-1} A_n \sin(K_n x - (\omega_n - K_n V)t + \phi_n) \\ &= \sum_{n=0}^{N_f-1} A_n \cos(K_n x - W_n t + \chi_n) \end{aligned} \quad (3)$$

where $A_n = \sigma C b^{(s-2)n}$, $K_n = K_0 b^n, W_n = \omega_n - K_n V$, $\chi_n = \phi_n - \pi/2$. Then we can apply the Lagrange model to establish the nonlinear fractal sea surface conveniently. For deep water, the nonlinear fractal sea surface can be written as [30–32]

$$\begin{aligned} f(x,t) = &\sum_{l=0}^{N_f-1} A_l \cos(K_l x - W_l t + \chi_l) + \frac{1}{2} K_{ave} \sum_{l=0}^{N_f-1} \sum_{m=0}^{N_f-1} A_l A_m \\ &\times \cos[(K_l + K_m)x - (W_l + W_m)t + \chi_l + \chi_m] + \frac{1}{2} K_{ave} \sum_{l=0}^{N_f-1} \sum_{m=0}^{N_f-1} \alpha_m A_l A_m \\ &\times \sin[(K_l + K_m)x - (W_l + W_m)t + \chi_l + \chi_m] \end{aligned} \quad (4)$$

where $\alpha_m = \xi/W_m^2$ and ξ is the parameter that donates the relation between the horizontal acceleration of water particles and vertical displacement and more detailed description can be find in [31, 32]. K_{ave} is the average wavenumber defined as

$$K_{ave} = \frac{\sum_{n=0}^{N_f-1} K_n A_n^2}{\sum_{n=0}^{N_f-1} A_n^2} \tag{5}$$

And also, the horizontal displacement of water particles can be expressed as

$$\begin{aligned} h(x,t) = &- \sum_{l=0}^{N_f-1} A_l \sin(K_l x - W_l t + \chi_l) + \sum_{l=0}^{N_f-1} \alpha_l A_l \sin(K_l x - W_l t + \chi_l) \\ &+ K_{ave} \sum_{l=0}^{N_f-1} \sum_{m=0}^{N_f-1} \alpha_l A_l A_m \cos[(K_l + K_m)x - (W_l + W_m)t + \chi_l + \chi_m] \\ &- \frac{1}{2} K_{ave} \sum_{l=0}^{N_f-1} \sum_{m=0}^{N_f-1} A_l A_m \sin[(K_l + K_m)x - (W_l + W_m)t + \chi_l + \chi_m] \\ &+ \frac{1}{2} K_{ave} \sum_{l=0}^{N_f-1} \sum_{m=0}^{N_f-1} \alpha_l \alpha_m A_l A_m \sin[(K_l + K_m)x - (W_l + W_m)t + \chi_l + \chi_m] \end{aligned} \tag{6}$$

The nonlinear fractal sea surface can be formed from (4) and (6). Figure 1 shows the linear and nonlinear fractal sea surface of wind

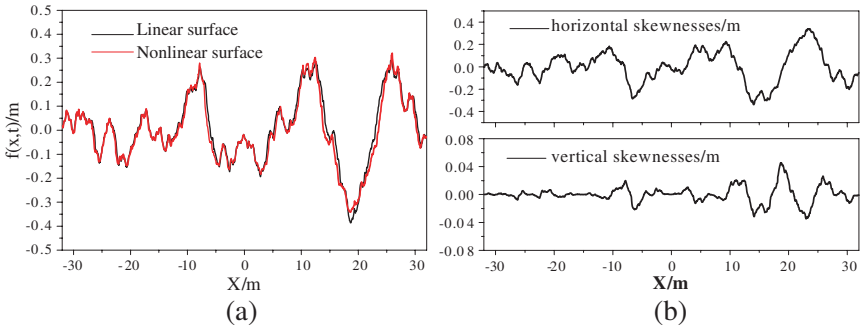

Figure 1. Linear and nonlinear fractal sea surface, (a) comparison of linear and nonlinear sea surface, (b) the horizontal and vertical skewness for nonlinear fractal sea surface.

speed 5 m/s. Figure 1(a) shows the comparison of linear and nonlinear sea surface, and Figure 1(b) shows the horizontal and vertical skewness of nonlinear sea surface. For simplicity, the platform velocity is set $V = 0$, and $\xi = 0.4$ is the same as in [32]. The fractal dimension $s = 1.1$, scale factor $b = 1.2$ and $N_f = 30$. $K_0 = 0.877^2 g/u$ and $C = 0.124u^2/4 \times 1.62$. From Figure 1, we can clearly see that the nonlinear sea surface will become steeper at wave crests and will become more flat at wave troughs.

3. SSA-II MODEL SCATTERING FROM ONE-DIMENSIONAL FRACTAL SEA SURFACE

In this section, the SSA-II model is employed to study the scattering of the fractal sea surface. The geometry of the scattering process is illustrated in Figure 2. θ_i and θ_s denote the incident angle and scattered angle. $\mathbf{k}_i$ is the incident wave vector and $\mathbf{k}_s$ is the scattering wave vector. They can be decomposed into horizontal and vertical components respectively.

$$\mathbf{k}_i = k_i\hat{\mathbf{x}} - q_i\hat{\mathbf{z}}, \quad \mathbf{k}_s = k_s\hat{\mathbf{x}} + q_s\hat{\mathbf{z}} \tag{7}$$

Suppose a tapered wave is incident on the sea surface and can be expressed as [37]

$$E_i(x,f) = G(x,f,\theta_i)\exp[-jk(x\sin\theta_i - f\cos\theta_i)] \tag{8}$$

$$G(x,f,\theta_i) = \exp\left[-\frac{(x+f\tan\theta_i)^2}{\nu^2} - j\frac{k(x\sin\theta_i - f\cos\theta_i)}{(k\nu\cos\theta_i)^2} \times \left(\frac{2(x+f\tan\theta_i)^2}{\nu^2} - 1\right)\right] \tag{9}$$

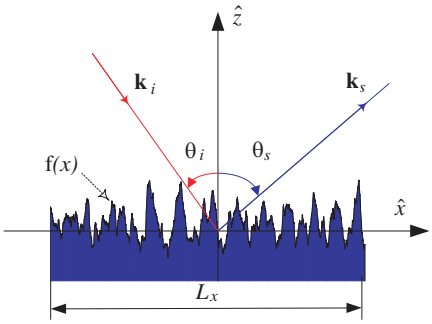

Figure 2. Geometry of the sea surface.

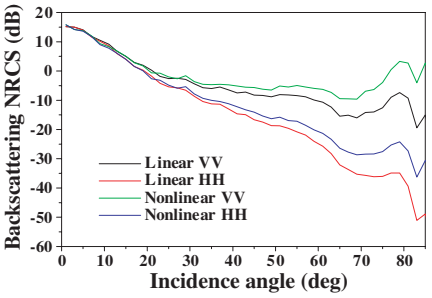

Figure 3. Backscattering NRCS versus incident angles.

where k donates the wavenumber of incidence wave, $G(x, f)$ is the taper function and ν is the parameter that controls the beam waist.

The scattering amplitude of SSA-II can be expressed as

$$\begin{aligned} S(\mathbf{k}_s, \mathbf{k}_i; t) \;=\; & \frac{2\sqrt{q_i q_s}}{(q_i + q_s)\sqrt{P_{inc}}} \int \frac{dx}{(2\pi)} G(x, f, \theta_i) \\ & \exp[-j(k_s - k_i)x + j(q_s + q_i) f(x,t)] \\ & \times \left[B(k_s, k_i) - \frac{j}{4} \int M(k_s, k_i; \zeta) F(\zeta, t) \exp(j\zeta x) d\zeta \right] \end{aligned} \quad (10)$$

where P_{inc} is the incident wave power, it can be expressed as

$$P_{inc} = \int |E_i(x, 0)|^2 \, dx \quad (11)$$

B and M can be found in [35], are dependent on configuration angles, the polarization, and the complex permittivity of sea surface. For simplicity, the expressions of B and M are given in Appendix A. $F(\zeta,\, t)$ is the Fourier transform of the sea surface elevation

$$F(\zeta, t) = \frac{1}{(2\pi)} \int f(x, t) \exp(-j\zeta x) dx \quad (12)$$

For the nonlinear fractal sea surface, the integral variables x in (10) should be replaced by $X = x + h(x, t)$ due to the horizontal displacement. Then the Jacobian J of the transformation from x to X is utilized to accomplish this change of integral variables. So Equation (10) should be rewritten as

$$\begin{aligned} S(\mathbf{k}_s, \mathbf{k}_i; t) = & \frac{2\sqrt{q_i q_s}}{(q_i + q_s)\sqrt{P_{inc}}} \int \frac{dx}{(2\pi)} G(x, f, \theta_i) \\ & \exp[-j(k_s - k_i)X + j(q_s + q_i) f(x,t)] \\ & \times J(x,t) \left[B(k_s, k_i) - \frac{j}{4} \int M(k_s, k_i; \zeta) H(\zeta, t) \exp(j\zeta x) d\zeta \right] \end{aligned} \quad (13)$$

where $J(x, t) = 1 + \partial h(x, t)/\partial x$. Then the average NRCS can be expressed as

$$\sigma_{\text{SSA-II}} = 4\pi q_i q_s \left\langle |S(\mathbf{k}_i, \mathbf{k}_s; t)|^2 \right\rangle \quad (14)$$

The nonlinearity affects not only the NRCS of sea surface, but also the Doppler spectrum of the sea clutter. And also, the Doppler analysis is a much more precise and sensitive tool for evaluating the validity of the scattering model than the NRCS, so the Doppler spectrum of sea clutter is of great interest for the remote sensing from the sea surface.

The Doppler spectrum is typically defined as the power spectral density of the time-evolving scattering amplitude and its expression is [38]

$$S_{\mathrm{Dop}}(f) = \left\langle \frac{1}{T} \left| \int_0^T S(k_s, k_i; t) \exp(-j2\pi f t) dt \right|^2 \right\rangle \tag{15}$$

The angle bracket denotes the ensemble average over much surface realizations. T is the duration of the sea surface evolution.

4. NUMERICAL RESULTS

4.1. Comparison of NRCS

In this section, the NRCS given by Equation (14) of wind speed 5 m/s is simulated, the frequency is 1.2 GHz, and the complex relative permittivity is $\varepsilon = 73.5 + j61.0$. The size of the sea surface is $L_x = 64$ m, the sample points is 2048, and the sample interval is $\lambda/8$. The parameter ν is chosen to be $L_x/6$. Each NRCS is obtained over 100 samples of sea surfaces.

The average backscattering NRCS versus incidence angles from linear and nonlinear surfaces is shown in Figure 3. It is seen that, the average NRCS of nonlinear surfaces is larger than its linear surface. At small incidence angles, the discrepancies are not large, and the discrepancies become larger with the increase of incidence angles, which indicates the nonlinearity is very important for sea surface scattering at low grazing angles. The differences value (DV) of NRCS between linear and nonlinear surfaces at incident angles of 9° and 81° are calculated, and the corresponding absolute percentage error (APE) are also included in Table 1. For bistatic case, the average NRCS versus scattering angles for incidence angles of 0° and 45° are shown in Figure 4. It can be seen from Figure 4, the discrepancies between linear and nonlinear surface are not large near the specular direction and the discrepancies become larger as the scattering angles departing

Table 1. DV and APE of NRCS at incident angles of 9° and 81° in Figure 3.

Incident angles	9°		81°	
	DV (dB)	APE (%)	DV (dB)	APE (%)
HH	0.6059	3.999	12.0276	30.0538
VV	0.6092	4.020	12.0237	129.3127

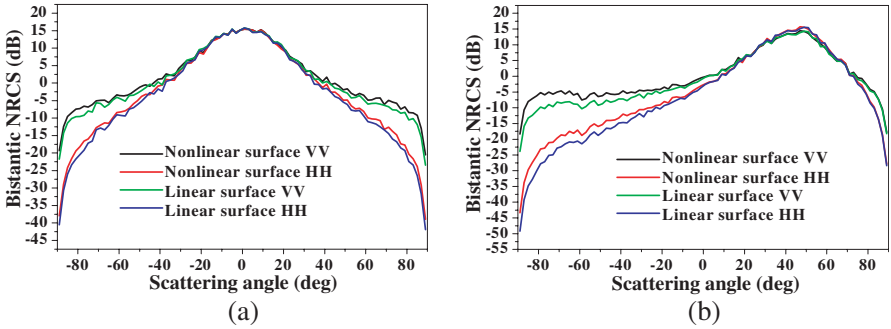

Figure 4. Bistatic NRCS versus scattering angles, (a) incidence angle of 0°, (b) incidence angle of 45°.

Table 2. DV and APE of NRCS at different scattering angles for 0° and 45° incident angle in Figure 4.

0° incident angle	Components	Scattering angle −89°		Scattering angle −1°	
		DV (dB)	APE (%)	DV (dB)	APE (%)
	HH	2.6215	6.463	0.0006	0.004
	VV	2.3813	10.944	0.0021	0.014
45° incident angle	Components	Scattering angle −89°		Scattering angle 45°	
		DV (dB)	APE (%)	DV (dB)	APE (%)
	HH	5.9039	11.993	0.3369	2.342
	VV	5.5022	23.089	0.3340	2.532

from the specular direction. The corresponding DV and APE of NRCS for different scattering angles are listed in Table 2.

4.2. Doppler Analysis

Compared with NRCS, the Doppler spectrum of sea surface backscattered signals is a more precise and sensitive tool for detecting to changes in the fluid motion. For deep water, the phase velocity of Bragg scattering can be written as

$$f_B(\theta_i) = \frac{1}{2\pi}\sqrt{2g_0 k \sin\theta_i} \tag{16}$$

where g_0 is the gravity acceleration. It is obvious that $f_B(\theta_i)$ is determined by the incidence angle and incidence frequency. However, the frequency shift and Doppler spectrum bandwidth of the measured Doppler spectrum is usually larger than the simulations from linear

sea surface, which is different from the Bragg theory. So it is necessary to consider the nonlinearity of sea surface.

In order to measure the characters of the Doppler spectrum, the Doppler shift f_s and the bandwidth of the Doppler spectrum f_w are employed to indicate the features of the linear and nonlinear fractal sea surfaces. Their expressions are given in [39]

$$f_s = \frac{\int f S_{Dop}(f)\, df}{\int S_{Dop}(f)\, df}, \quad f_w^2 = \frac{\int (f - f_s)^2 S_{\mathrm{Dop}}(f)\, df}{\int S_{\mathrm{Dop}}(f)\, df} \tag{17}$$

Figure 5 shows the Doppler spectrum for different incidence angles of a wind speed of 5 m/s, and Figure 7 shows the Doppler spectra of

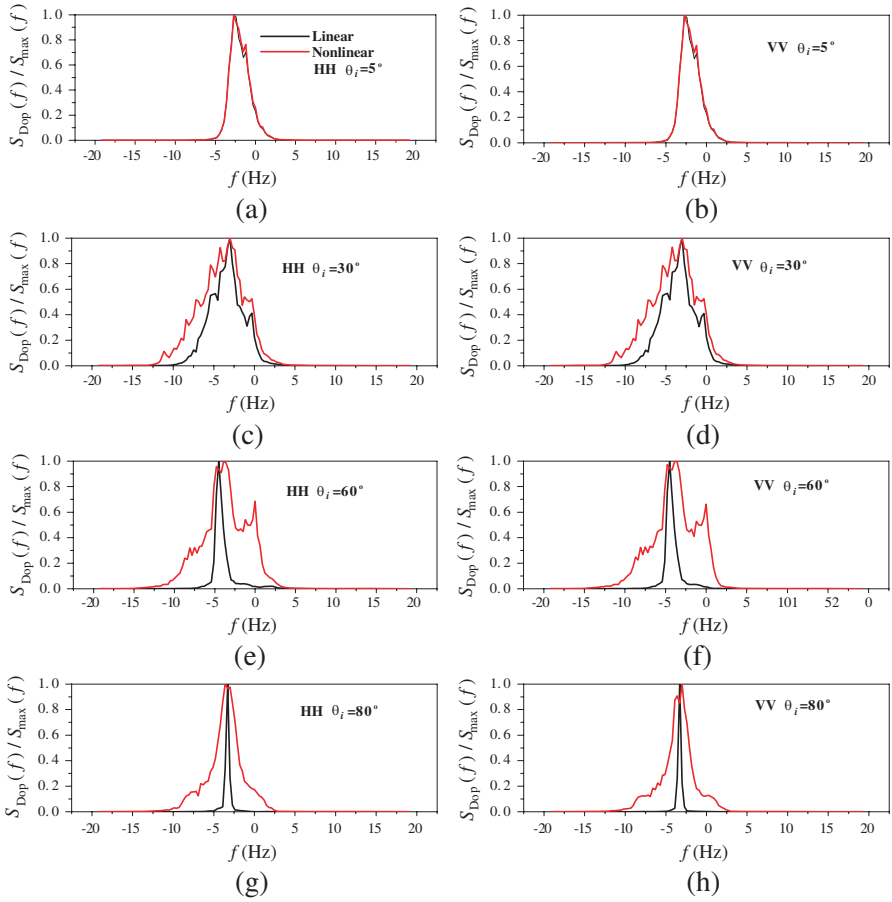

Figure 5. The normalized Doppler spectra of linear surfaces and the nonlinear surfaces, $s = 1.1$, wind speed 5 m/s.

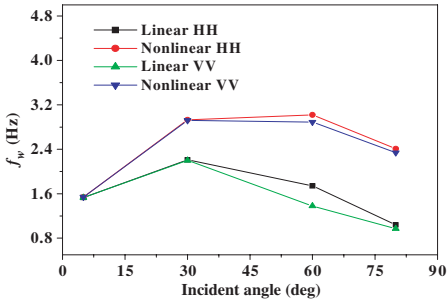

Figure 6. The bandwidths of the Doppler spectra at different incident angles for wind speed 5 m/s.

a larger fractal dimension $s = 1.4$ for 5 m/s and 7 m/s at $\theta_i = 80°$. For 5 m/s, the size of the sea surface is the same as above $L_x = 64$ m, and the size of sea surface is $L_x = 128$ m for 7 m/s. The time step is 0.02 s, and each spectral realization is performed on 128 samples. The average spectrum is obtained from 100 realizations. It can be seen from Figure 5, the Doppler spectra for linear and nonlinear fractal sea surfaces coincide with each other at small incident angles. When the incident angle increases, the bandwidths of Doppler spectra firstly increase and then decrease both for linear and nonlinear surfaces. This effect is clearly observed in Figure 6 where the corresponding Doppler spectra bandwidths are shown. These are similar with the results of stochastic wave sea surfaces in [27, 40]. In Figure 6, if the largest incident angle, for example $\theta_i = 80°$, is considered, it can be seen that the bandwidths of nonlinear surfaces can reach as large as 2.4 Hz while the bandwidths of linear surfaces are just about 1.0 Hz. This is due to the fact that the nonlinear-wave components propagate faster than the linear-wave components.

Compared with the result $s = 1.1$, the Doppler spectrum has larger bandwidth in Figures 7(a) and (b) for wind speed 5 m/s, $s = 1.4$ at $\theta_i = 80°$, which is caused by the increased roughness of fractal sea surface. The Doppler shifts and bandwidths corresponding Figure 7 are listed in Table 3. From Table 3, we can see that the nonlinearity has a large influence on the bandwidths, while the influence on the Doppler shifts is little for wind speed 5 m/s. And the nonlinearity not only has a large influence on the bandwidths, but also has a great influence on the Doppler shifts under wind speed 7 m/s. And also, he peak frequencies in Figures 7(c) and (d) for 7 m/s can reach relative large values (HH -7.2 Hz, VV -7.2 Hz), while the values (HH -3.3 Hz, VV -3.0 Hz) in Figures 7(a) and (b) for 5 m/s is smaller. This is attributed to the fact that the nonlinear fractal sea surface corrects the phase velocities

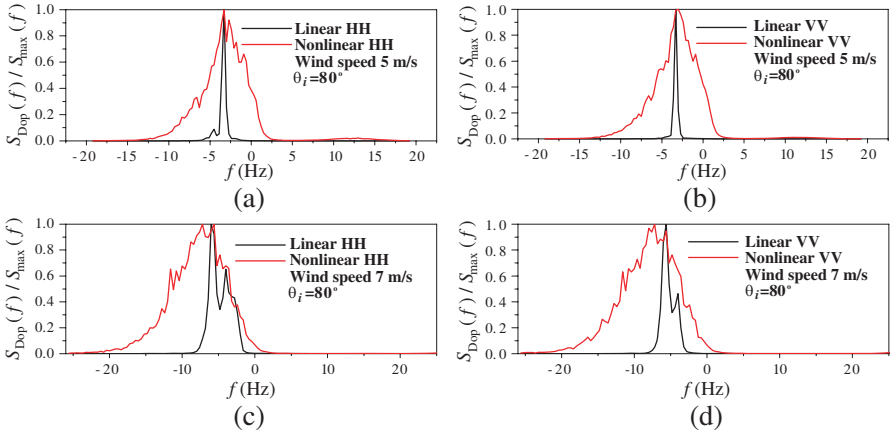

Figure 7. Doppler spectrum of $s = 1.4$, (a), (b) wind speed of 5 m/s, (c), (d) wind speed of 7 m/s.

Table 3. The bandwidths of the Doppler spectra and Doppler shifts in Figure 7.

Bandwidths	$S = 1.4, 5$ m/s		$S = 1.4, 7$ m/s	
	Linear	Nonlinear	Linear	Nonlinear
HH (Hz)	1.1101	3.6702	1.8056	4.1497
VV (Hz)	0.9481	3.1991	1.4822	4.3045
Shifts	Linear	Nonlinear	Linear	Nonlinear
HH (Hz)	−3.4497	−3.1070	−4.7148	−7.8185
VV (Hz)	−3.3232	−3.2652	−5.2797	−8.0025

by adding the horizontal and vertical skewness, and the influence of nonlinearity increases with the increasing of wind speed.

5. CONCLUSION

In this paper, a one-dimensional nonlinear fractal sea surface model has been established based on the narrow-band Lagrange model. Analyzed by SSA-II, the NRCS and Doppler spectrum of linear and nonlinear fractal sea surface is calculated. The NRCS of nonlinear sea surface is larger than the linear sea surface for backscattering, especially for large incidence angles. And for bistatic case, the result of nonlinear sea surface is also larger than the linear fractal sea surface,

which is characterized as the discrepancies being small near specular direction, while the discrepancies becoming larger as the scattering angles departing from the specular direction. These indicate the nonlinearity of sea surface has important influence on the scattering echoes of sea surface, especially for large incidence angles and large scattering angles. For Doppler spectrum, at small incidence angles, the differences between nonlinear and linear surface is not obvious. As the increase of incidence angles, the nonlinearity of sea surface effects greatly enhances the Doppler shift and the Doppler spectrum bandwidth. These are attributed the fact that the nonlinear-wave components propagate faster than the linear-wave components and the nonlinear fractal sea surface corrects the phase velocities by adding the horizontal and vertical skewness. All the result shows the validity of this nonlinear model.

The scattering results in this paper from the nonlinear fractal sea surface model can help to better understand the scattering from fractal sea surface, especially for the time-dependent signals, though the fractal sea surface is limited to one-dimension. And also, this nonlinear fractal sea surface model might be applicable to establish a two-dimensional nonlinear fractal sea surface, which can potentially provide a higher precision RCS and Doppler spectrum in studies of electromagnetic scattering from the sea surfaces.

ACKNOWLEDGMENT

The authors would like to thank the Fundamental Research Funds for the Central Universities, the National Natural Science Foundation of China under Grant No. 60871070, and the Foundation of the Science and Technology on Electromagnetic Scattering Laboratory to support this kind of research.

APPENDIX A.

The general expressions for kernel functions B and M based on vertically and horizontally polarized waves are given in [35]. The first order B can be expressed as:

$$B_{VV}\left(\vec{k},\vec{k}_0\right)=\frac{\varepsilon-1}{\left(\varepsilon q_k^{(1)}+q_k^{(2)}\right)\left(\varepsilon q_0^{(1)}+q_0^{(2)}\right)}\left(q_k^{(2)}q_0^{(2)}\frac{\vec{k}\cdot\vec{k}_0}{kk_0}-\varepsilon kk_0\right) \quad \text{(A1)}$$

$$B_{VH}\left(\vec{k},\vec{k}_0\right)=\frac{\varepsilon-1}{\left(\varepsilon q_k^{(1)}+q_k^{(2)}\right)\left(q_0^{(1)}+q_0^{(2)}\right)}\frac{\omega}{c}q_k^{(2)}\frac{\vec{k}\times\vec{k}_0}{kk_0} \tag{A2}$$

$$B_{HV}\left(\vec{k},\vec{k}_0\right)=\frac{\varepsilon-1}{(q_k^{(1)}+q_k^{(2)})\left(\varepsilon q_0^{(1)}+q_0^{(2)}\right)}\frac{\omega}{c}q_0^{(2)}\frac{\vec{k}\times\vec{k}_0}{kk_0} \tag{A3}$$

$$B_{HH}\left(\vec{k},\vec{k}_0\right)\ =\ -\frac{\varepsilon-1}{\left(q_k^{(1)}+q_k^{(2)}\right)\left(q_0^{(1)}+q_0^{(2)}\right)}\frac{\omega^2}{c^2}\frac{\vec{k}\cdot\vec{k}_0}{kk_0} \tag{A4}$$

The second order M can be expressed as:

$$\begin{aligned}M_{VV}\left(\vec{k},\vec{k}_0,\vec{\xi}\right)=&\frac{\varepsilon-1}{\left(\varepsilon q_k^{(1)}+q_k^{(2)}\right)\left(\varepsilon q_0^{(1)}+q_0^{(2)}\right)}\left[-2\frac{\varepsilon-1}{\varepsilon q_\xi^{(1)}+q_\xi^{(2)}}\left(q_k^{(2)}q_0^{(2)}\frac{\vec{k}\cdot\vec{\xi}}{k}\frac{\vec{\xi}\cdot\vec{k}_0}{k_0}\right.\right.\\&\left.+\varepsilon kk_0\xi^2\right)+2\varepsilon\frac{q_\xi^{(1)}+q_\xi^{(2)}}{\varepsilon q_\xi^{(1)}+q_\xi^{(2)}}\left(k_0q_k^{(2)}\frac{\vec{k}\cdot\vec{\xi}}{k}+kq_0^{(2)}\frac{\vec{\xi}\cdot\vec{k}_0}{k_0}\right)\\&\left.-\left(\varepsilon\frac{\omega^2}{c^2}(q_k^{(2)}+q_0^{(2)}\right)+2q_k^{(2)}q_0^{(2)}\left(q_\xi^{(1)}-q_\xi^{(2)}\right)\right)\frac{\vec{k}\cdot\vec{k}_0}{kk_0}\right]\end{aligned} \tag{A5}$$

$$\begin{aligned}M_{VH}\left(\vec{k},\vec{k}_0,\vec{\xi}\right)=&\frac{(\varepsilon-1)\omega/c}{\left(\varepsilon q_k^{(1)}+q_k^{(2)}\right)\left(q_0^{(1)}+q_0^{(2)}\right)}\\&\left[-2\frac{\varepsilon-1}{\varepsilon q_\xi^{(1)}+q_\xi^{(2)}}q_k^{(2)}\frac{\vec{k}\cdot\vec{\xi}}{k}\frac{\vec{\xi}\times\vec{k}_0}{k_0}+2\varepsilon\frac{q_\xi^{(1)}+q_\xi^{(2)}}{\varepsilon q_\xi^{(1)}+q_\xi^{(2)}}k\frac{\vec{\xi}\times\vec{k}_0}{k_0}\right.\\&\left.-\left(\varepsilon\frac{\omega^2}{c^2}+q_k^{(2)}q_0^{(2)}+2q_k^{(2)}\left(q_\xi^{(1)}-q_\xi^{(2)}\right)\right)\frac{\vec{k}\times\vec{k}_0}{kk_0}\right]\end{aligned} \tag{A6}$$

$$\begin{aligned}M_{HV}=&\frac{(\varepsilon-1)\omega/c}{\left(q_k^{(1)}+q_k^{(2)}\right)\left(\varepsilon q_0^{(1)}+q_0^{(2)}\right)}\\&\left[2\frac{\varepsilon-1}{\varepsilon q_\xi^{(1)}+q_\xi^{(2)}}q_0^{(2)}\frac{\vec{k}_0\cdot\vec{\xi}}{k_0}\frac{\vec{\xi}\times\vec{k}}{k}-2\varepsilon\frac{q_\xi^{(1)}+q_\xi^{(2)}}{\varepsilon q_\xi^{(1)}+q_\xi^{(2)}}k_0\frac{\vec{\xi}\times\vec{k}}{k}\right.\\&\left.-\left(\varepsilon\frac{\omega^2}{c^2}+q_k^{(2)}q_0^{(2)}+2q_0^{(2)}\left(q_\xi^{(1)}-q_\xi^{(2)}\right)\right)\frac{\vec{k}\times\vec{k}_0}{kk_0}\right]\end{aligned} \tag{A7}$$

$$M_{HH}=\frac{(\varepsilon-1)}{\left(q_k^{(1)}+q_k^{(2)}\right)\left(q_0^{(1)}+q_0^{(2)}\right)}\frac{\omega^2}{c^2}\left[-2\frac{\varepsilon-1}{\varepsilon q_\xi^{(1)}+q_\xi^{(2)}}\left(\frac{\vec{k}\cdot\vec{\xi}}{k}\frac{\vec{k}_0\cdot\vec{\xi}}{k_0}-\xi^2\frac{\vec{k}\cdot\vec{k}_0}{kk_0}\right)\right.$$
$$\left.+\left(q_k^{(2)}+q_0^{(2)}+2\left(q_\xi^{(1)}-q_\xi^{(2)}\right)\right)\frac{\vec{k}\cdot\vec{k}_0}{kk_0}\right] \quad \text{(A8)}$$

where $\vec{k}$ and $\vec{k}_0$ donate the horizontal wavevector of scattered wave and incident wave, respectively. In this paper, $\vec{k}$, $\vec{k}_0$ and $\vec{\xi}$ just need to be replaced by k_s, k_i, and ζ. ε is the complex relative permittivity of sea water, and c is the speed of light. $q_k^{(1,2)}$ and $q_0^{(1,2)}$ are the vertical components of the wavevectors, and can be expressed as:

$$q_k^{(1)}=\sqrt{\frac{\omega^2}{c^2}-k^2} \quad q_k^{(2)}=\sqrt{\varepsilon\frac{\omega^2}{c^2}-k^2} \quad \mathrm{Im}q_k^{(1)},\ q_k^{(2)}>0 \quad \text{(A9)}$$

$$q_0^{(1)}=\sqrt{\frac{\omega^2}{c^2}-k_0^2} \quad q_k^{(2)}=\sqrt{\varepsilon\frac{\omega^2}{c^2}-k_0^2} \quad \mathrm{Im}q_0^{(1)},\ q_0^{(2)}>0 \quad \text{(A10)}$$

REFERENCES

1. Baussard, A., M. Rochdi, and A. Khenchaf, "PO/Mec-based scattering model for complex objects on a sea surface," *Progress In Electromagnetics Research*, Vol. 111, 229–251, 2011.
2. Kurrant, D. J. and E. C. Fear, "Extraction of internal spatial features of inhomogeneous dielectric objects using near-field reflection data," *Progress In Electromagnetics Research*, Vol. 122, 197–221, 2012.
3. Ji, W.-J. and C.-M. Tong, "Bistatic scattering from two-dimensional dielectric ocean rough surface with a PEC object partially embedded by using the G-SMCG method," *Progress In Electromagnetics Research*, Vol. 105, 119–139, 2010.
4. Chen, H., M. Zhang, and H.-C. Yin, "Facet-based treatment on microwave bistatic scattering of three-dimensional sea surface with electrically large ship," *Progress In Electromagnetics Research*, Vol. 123, 385–405, 2012.
5. Yang, W., Z. Zhao, C. Qi, W. Liu, and Z.-P. Nie, "Iterative hybrid method for electromagnetic scattering from a 3-D object above a 2-D random dielectric rough surface," *Progress In Electromagnetics Research*, Vol. 117, 435–448, 2011.
6. Luo, W., M. Zhang, Y. W. Zhao, and H. Chen, "An efficient hybrid high-frequency solution for the composite scattering of

the ship very large two-dimensional sea surface," *Progress In Electromagnetics Research M*, Vol. 8, 79–89, 2009.

7. Zhang, M., W. Luo, G. Luo, C. Wang, and H.-C. Yin, "Composite Scattering of ship on sea surface with breaking waves," *Progress In Electromagnetics Research*, Vol. 123, 263–277, 2012.
8. Wu, Z.-S., J.-J. Zhang, and L. Zhao, "Composite electromagnetic scattering from the plate target above a one-dimensional sea surface: Taking the diffraction into account," *Progress In Electromagnetics Research*, Vol. 92, 317–331, 2009.
9. Chang, Y.-L., C.-Y. Chiang, and K.-S. Chen, "SAR image simulation with application to target recognition," *Progress In Electromagnetics Research*, Vol. 119, 35–57, 2011.
10. Chen, H., M. Zhang, D. Nie, and H.-C. Yin, "Robust semi-deterministic facet model for fast estimation on EM scattering from ocean-like surface," *Progress In Electromagnetics Research B*, Vol. 18, 347–363, 2009.
11. Nie, D. and M. Zhang, "Bistatic scattering analysis for two-dimensional rough sea surfaces using an angular composite model," *Int. J. Remote Sens.*, Vol. 32, No. 24, 9661–9672, 2011.
12. Huang, C.-W. and K. C.-Lee, "Application of ICA technique to PCA based radar target recognition," *Progress In Electromagnetics Research*, Vol. 105, 157–170, 2010.
13. Zhang, M., Y. W. Zhao, H. Chen, and W.-Q. Jiang, "SAR imaging simulation for composite model of ship on dynamic ocean scene," *Progress In Electromagnetics Research*, Vol. 113, 395–412, 2011.
14. Liang, D., P. Xu, L. Tsang, Z. Gui, and K.-S. Chen, "Electromagnetic scattering by rough surfaces with large heights and slopes with applications to microwave remote sensing of rough surface over layered media," *Progress In Electromagnetics Research*, Vol. 95, 199–218, 2009.
15. Guo, L.-X., Y. Liang, J. Li, and Z.-S, Wu, "A high order integral SPM for the conducting rough surface scattering with the tapered wave incidence-TE case," *Progress In Electromagnetics Research*, Vol. 114, 333–352, 2011.
16. Mandelbrot, B. B., *The Fractal Geometry of Nature*, W. H. Freeman, San Francisco, 1982.
17. Jakeman, E., "Fresnel scattering by a corrugated random surface with fractal slope," *J. Opt. Soc. Am.*, Vol. 72, No. 8, 1034–1041, 1982.
18. Berizzi, F., E. D. Mese, and G. Pinelli, "One-dimensional fractal model of the sea surface," *IEE Proc. Radar, Sonar Navig.*,

Vol. 146, No. 1, 55–64, 1999.

19. Guo, L.-X. and Z.-S. Wu, "Fractal model and electromagnetic scattering from time-varying sea surface," *Electr. Lett.*, Vol. 36, No. 21, 1801–1812, 2000.
20. Berizzi, F., M. Greco, and L. Verrazzani, "Fractal approach for sea clutter generation," *IEE Proc. Radar, Sonar Navig.*, Vol. 147, No. 4, 189–198, 2000.
21. Liu, W., L.-X. Guo, and Z.-S. Wu, "Polarimetric scattering from a two-dimensional improved sea fractal surface," *Chin. Phys. B*, Vol. 19, No. 7, 074012-1, 2010.
22. Berizzi, F. and E. D. Mese, "Scattering coefficient evaluation from a two-dimensional sea fractal surface," *IEEE Trans. on Antennas and Propagat.*, Vol. 50, No. 4, 426–434, 2002.
23. Chen, J., et al., "The use of fractals for modeling EM waves scattering from rough sea surface," *IEEE Trans. on Geosci. Remote Sens.*, Vol. 34, No. 4, 966–972, 1996.
24. Xie, T., et al., "Numerical study of electromagnetic scattering from one-dimensional nonlinear fractal sea surface," *Chin. Phys. B*, Vol. 19, No. 2, 024101-1, 2010.
25. Guo, L. and C. Kim, "Study on the two-frequency scattering cross section and pulse broadening of the one-dimensional fractal sea surface at millimeter wave frequency," *Progress In Electromagnetics Research*, Vol. 37, 221–234, 2002.
26. Xie, T., et al., "A two scale nonlinear fractal sea surface model in a one dimensional deep sea," *Chin. Phys. B*, Vol. 19, No. 5, 059201-1, 2010.
27. Li, X.-F. and X.-J. Xu, "Scattering and Doppler spectral analysis for two-dimensional linear and nonlinear sea surfaces," *IEEE Trans. on Geosci. Remote Sens.*, Vol. 49, No. 2, 603–611, 2011.
28. Nouguier, F., C. A. Guérin, and G. Soriano, "Analytical techniques for the Doppler signature of sea surfaces in the microwave regime. II: Nonlinear surfaces," *IEEE Trans. on Geosci. Remote Sens.*, Vol. 49, No. 12, 4920–4927, 2011.
29. Johnson, J. T., J. V. Toporkov, and G. S. Brown, "A numerical study of backscattering from time-evolving sea surfaces: Comparison of hydrodynamic models," *IEEE Trans. on Geosci. Remote Sens.*, Vol. 39, No. 11, 2411–2420, 2001.
30. Lindgren, G. and S. Aberg, "First order stochastic Lagrange model for asymmetric ocean waves," *J. Offshore Mech. Arct. Eng.*, Vol. 131, No. 3, 031602, 2009.
31. Lindgren, G., "Exact asymmetric slope distributions in stochastic

gauss Lagrange ocean waves," *Appl. Ocean Res.*, Vol. 31, No. 1, 65–73, 2009.

32. Wang, Y.-H., Y.-M. Zhang, M.-X. He, and C.-F. Zhao, "Doppler spectra of microwave scattering fields from nonlinear oceanic surface at moderate- and low-grazing angles," *IEEE Trans. on Geosci. Remote Sens.*, Vol. 50, No. 4, 1104–1116, 2012.
33. Voronovich, A. G., "Small-slope approximation in wave scattering by rough surface," *Sov. Phys. JETP*, Vol. 62, 65–70, 1985.
34. Voronovich, A. G., "Small-slope approximation for electromagnetic wave scattering at a rough interface of two dielectric half-spaces," *Wave Random Media*, Vol. 4, 337–367, 1994.
35. Voronovich, A. G. and V. U. Zavorotny, "Theoretical model for scattering of radar signals in Ku- and C-bands from a rough sea surface with breaking waves," *Waves Random Media*, Vol. 11, No. 3, 247–269, 2001.
36. Berizzi, F. and E. D. Mese, "Fractal analysis of the signal scattered from the sea surface," *IEEE Trans. on Geosci. Remote Sens.*, Vol. 47, No. 2, 324–338, 1999.
37. Tsang, L., J. A. Kong, and K. H. Ding, *Scattering of Electromagnetic Waves*, John Wiley & Sons Inc., New York, 2001.
38. Toporkov, J. V. and G. S. Brown, "Numerical simulation of scattering from time-varying, randomly rough surfaces," *IEEE Trans. on Geosci. Remote Sens.*, Vol. 38, No. 4, 1616–1625, 2000.
39. Toporkov, J. V., M. A. Sletten, and G. S. Brown, "Numerical scattering simulations from time-evolving ocean-like surfaces at L- and X-band: Doppler analysis and comparisons with a composite surface analytical model," *Proc. Gen. Assem. Int. URSI*, Maastricht, The Netherlands, 2002.
40. Nie, D., M. Zhang, X. Geng, and P. Zhou, "Investigation on Doppler spectral characteristics of electromagnetic backscattered echoes from dynamic nonlinear surfaces of finite-depth sea," *Progress In Electromagnetics Research*, Vol. 130, 169–186, 2012.